

A FRET-Based Sensor Reveals Large ATP Hydrolysis-Induced Conformational Changes and Three Distinct States of the Molecular Motor Myosin

William M. Shih,* Zygmunt Gryczynski,†
Joseph R. Lakowicz,† and James A. Spudich*‡

*Department of Biochemistry
Stanford University School of Medicine
Stanford, California 94305

†Center for Fluorescence Spectroscopy
Department of Biochemistry
University of Maryland School of Medicine
Baltimore, Maryland 21201

Summary

The molecular motor myosin is proposed to bind to actin and swing its light-chain binding region through a large angle to produce an ~ 10 nm step in motion coupled to changes in the nucleotide state at the active site. To date, however, direct dynamic measurements have largely failed to show changes of that magnitude. Here, we use a cysteine engineering approach to create a high resolution, FRET-based sensor that reports a large, ~ 70 degree nucleotide-dependent angle change of the light-chain binding region. The combination of steady-state and time-resolved fluorescence resonance energy transfer measurements unexpectedly reveals two distinct prestroke states. The measurements also show that bound Mg.ADP.P_i, and not bound Mg.ATP, induces the myosin to adopt the prestroke states.

Introduction

The myosin molecular motor uses the energy of Mg.ATP hydrolysis to power the vectorial transport of adjacent actin filaments. A swinging crossbridge model of contraction was proposed by H. E. Huxley (1969) based on low-angle X-ray diffraction and electron microscope studies of muscle. A cycle of actin–myosin interactions is thought to occur as follows (Lyman and Taylor, 1971; Spudich, 1994): the myosin crossbridge binds to ATP, and then releases its attached actin filament. Next, the myosin crossbridge hydrolyzes the ATP and primes itself in preparation for a productive working stroke. Actin rebinding triggers phosphate release, which in turn prompts the myosin crossbridge to return to its starting conformation, in a motion termed the “powerstroke.” The net result is that the attached actin filament gets translocated in the direction of its minus (pointed) end. The myosin crossbridge is the subfragment 1 (S1) domain, which consists of the actin binding and nucleotide binding globular catalytic domain and the ~ 10 nm long light chain binding region (Figure 1). Crystal structures of monomeric actin (Kabsch et al., 1990) and myosin S1 (Rayment et al., 1993), combined with electron micrographic reconstructions of actin filaments with and without S1 decoration (Holmes et al., 1990; Rayment et al.,

1993; Schroder et al., 1993), provided strong support for a modification of this model that involves a relatively fixed catalytic domain bound to actin and swinging of the light chain binding region through a considerable angle, providing a working stroke of 5–15 nm (Cooke, 1986; Spudich, 1994). Thus, the light chain binding region of S1 is thought to act like a lever arm to amplify smaller conformational changes in S1 near the nucleotide binding site. Mg.ATP binding to S1 and its hydrolysis releases the myosin from the actin and regenerates the prestroke state of the myosin head for a subsequent working stroke. Actin rebinding stimulates phosphate release, which triggers the power stroke.

More recently, crystal structures have been solved for various truncated isoforms of myosin-II head fragments complexed with nucleotides (Fisher et al., 1995; Smith and Rayment, 1996; Dominguez et al., 1998; Houdusse et al., 1999). Relative to the globular catalytic domain, the carboxy-terminal converter domain has been found in five angular positions whose extremes place the lever arm domain pointing in almost opposite directions. Furthermore, the light chain bound α -helical lever arm has been found with or without a bend immediately distal to the converter domain (Rayment et al., 1993; Houdusse et al., 1999). Two themes that emerge from consideration of these structures are as follows: (1) Crystal structures that have been proposed as models of a prestroke state imply a step size of ~ 10 nm in magnitude, and (2) the lever arm may have the potential to stably adopt more than two different angles.

It is critical to test the validity of these structural themes for myosin outside the context of a crystal lattice, both in muscle fibers and in purified protein systems. Can the conformations seen by crystallography be detected under dynamic and more physiological conditions? Can additional conformations not yet seen by crystallography be resolved by other methods? Cryoelectron microscopic studies on actin filaments decorated with certain isoforms of myosin S1 suggest a small rotation of the lever arm domain upon release of ADP, thus implying two poststroke like conformations of myosin (Jontes et al., 1995; Whittaker et al., 1995). In a recent tomographic three-dimensional reconstruction study on quick-frozen contracting insect flight muscle, the authors interpreted tomographic images in terms of twenty six rebuilt S1s, for which the angle between the lever arm domain and the catalytic domain varied continuously in a range of $\sim 50^\circ$, where the rigor structure was placed near the middle of that range (Taylor et al., 1999). Thus, none of the rebuilt S1s exhibited a lever arm to catalytic domain angle similar to the crystallographic prestroke state models ($\sim 70^\circ$ – 80° away from the rigor angle).

An important approach to measuring conformational changes in proteins is the use of reporter probes attached to the purified protein that allow readout of dynamic changes in structure in response to changing conditions of environment. Dynamic measurements of changes in the myosin head structure, for example, have involved the use of various probes that report changes

‡ To whom correspondence should be addressed (e-mail: jspudich@cmgm.stanford.edu).

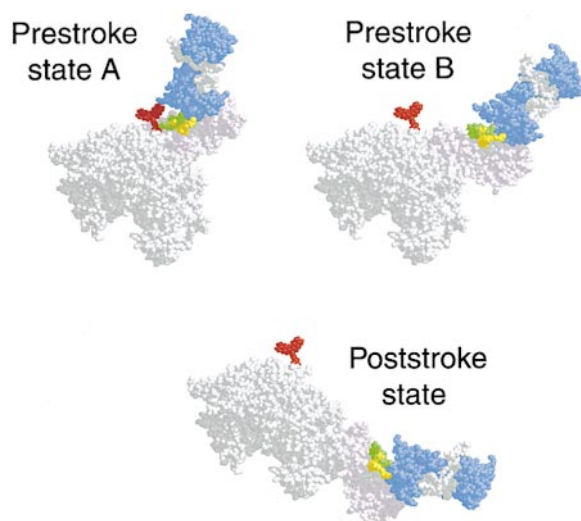


Figure 1. View of Doubly Labeled Myosin-II S1 with Three Proposed Lever Arm Angles

The heavy chain (HC) is colored white, the essential light chain (ELC) is colored light violet, and the regulatory light chain (RLC) is colored blue. Tetramethylrhodamine-5-maleimide (the acceptor dye) attached to HC-Cys₂₅₀ is colored red, and Oregon green 488 maleimide (the donor dye) is colored green or yellow according to its attachment to the RLC at either RLC-Cys₁₁₄ or RLC-Cys₁₁₆ (residues 113 and 115 in the chicken skeletal sequence), respectively. The distance between the donor and acceptor dyes decreases dramatically in going from the poststroke to the prestroke states, leading to a large increase in FRET efficiency.

in S1 structure in different nucleotide states. Such measurements have provided support for structural changes, but have often been hampered by restrictions as to where the probe can be placed on the molecule. Thus, a wide variety of angle changes of the lever arm have been estimated by these dynamic approaches (for review, see Goldman, 1998). Studies observing polarized fluorescence of rabbit muscle labeled on the regulatory light chain (Irving et al., 1995; Corrie et al., 1999) suggest at least a modest change in lever arm angle upon binding and hydrolysis of ATP, while EPR studies on spin-labeled myosin heads suggest dynamic disorder in the angle between the catalytic domain and lever arm in relaxed and active muscle (Roopnarine et al., 1998). Resonance energy transfer measurements between fluorescent or luminescent probes on the catalytic domain and the regulatory light chain have also indicated nucleotide-induced rotation of the lever arm (Burmeister-Getz et al., 1998; Xiao et al., 1998; Palm et al., 1999). A steady-state FRET study on a *Dictyostelium* catalytic domain in the absence of the light chain binding domain involved engineering green fluorescent protein onto the amino terminus and blue fluorescent protein onto the carboxy terminus. This study was consistent with a large angle change in the converter domain, from which the lever arm domain extends (Suzuki et al., 1998). Crystallographic studies (Houdusse et al., 1999) have shown, however, that the absence of the essential light chain can lead to a different conformation of the converter domain, and the location of the carboxy terminus in different nucleotide states may not reflect the relative

changes of the true lever arm with respect to the catalytic domain of the S1.

In addition to the question of the extent of a lever arm angle change, there has been considerable debate about whether myosin S1 discriminates between Mg.ATP and Mg.ADP.P_i in terms of lever arm conformations (Lymn and Taylor, 1971; Eisenberg and Greene, 1980; Fisher et al., 1995; Holmes, 1997; Dominguez et al., 1998; Huxley, 1998; Suzuki et al., 1998; Brust-Mascher et al., 1999; Houdusse et al., 1999). Crystal structures of myosin fragments complexed with the presumed Mg.ATP analog Mg.ADP.BeF_x have been found in both poststroke and prestroke angles, depending on the context (Fisher et al., 1995; Houdusse et al., 1999). Mutants of the *Dictyostelium* myosin catalytic domain have been found that bind weakly to actin when complexed to Mg.ATP, but which exhibit either prestroke- or poststroke-like angles of the converter domain (Sasaki et al., 1998; Suzuki et al., 1998). Thomas and colleagues have argued based on EPR data that S1 does not discriminate between ATP and ADP.P_i (Brust-Mascher et al., 1999). Answering this question and determining the extent of lever arm angle change requires the development of a reliable assay for the lever arm angle in the Mg.ATP state and in the Mg.ADP.P_i state. Dynamic approaches to date have usually involved putting probes on the myosin head where possible, given the structure and sequence of the native protein. Ideally, a myosin motor domain needs to be created that allows one to put probes at any site one chooses, to optimally assess the conformational change that one wishes to measure.

To achieve this goal, we have used cysteine engineering to remove native cysteines present in *Dictyostelium* myosin-II, and have shown that this cysteine-light myosin-II is functional both in vitro and in vivo. We then inserted cysteine residues in specific locations of *Dictyostelium* myosin-II S1 (Manstein et al., 1989). Specific labeling of those introduced cysteines with a donor and acceptor dye provided a FRET-based sensor capable of resolving a wide range of lever arm angles. This approach—removal of native cysteines and introduction of new cysteines at rationally selected positions on two separate polypeptides—helps circumvent problems of labeling specificity, perturbation of activity, and/or limited sensitivity to conformational changes that are often encountered with FRET studies. To accurately resolve the FRET distances, we measured a combination of steady-state and time-resolved FRET efficiencies. The measurements reported here unexpectedly indicate two prestroke conformations, one of which has not been seen yet crystallographically. In addition, we observe that bound ADP.P_i biases S1 toward prestroke states much more than does bound ATP.

Results and Discussion

Generation of a *Dictyostelium* Cysteine-Light Myosin-II: Design of the Substitutions

The paramount concern for mutagenizing myosin to remove cysteines was to retain function of the enzyme. We used the information that the cysteine residue demonstrates a tolerance for substitution with small and medium sized hydrophobic residues such as alanine,

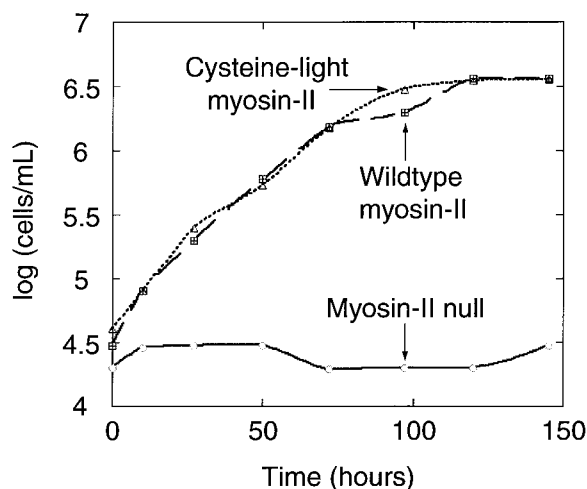


Figure 2. *Dictyostelium* Growth in Suspension

Growth is plotted as the log of the number of cells per ml versus time. The growth of cells lacking the myosin-II gene is rendered with open circles and a solid line, the growth of cells with a wild-type myosin-II gene is rendered with tetrasectioned open squares and a dashed line, and the growth of cells with a cysteine-light myosin-II gene is rendered with a dotted line and open triangles.

valine, isovaline, leucine, and isoleucine, as well as with serine, threonine, and tyrosine (Dayhoff, 1978). Sequence alignments of the myosin-IIs provided more information about which substitutions might be tolerated (Sellers and Goodson, 1995). Furthermore, the trends in the sequence alignment were compared with the environment of these residues in the crystal structures that have been solved. For cysteine 312, for example, the sequence alignment shows a strong predisposition toward tyrosine and phenylalanine. The structure shows that one face of cysteine 312 is surface exposed. For cysteine 470, the sequence alignment shows that cysteine is fairly well conserved, with some substitutions of tryptophan, isoleucine, valine, methionine, and lysine. The crystal structure shows that cysteine 470 appears well buried, consistent with the sequence alignment. For cysteine 655, the sequence alignment shows cysteine used almost exclusively. Cysteine 655 is the most conserved of the cysteines in *Dictyostelium* myosin-II. The structure shows that cysteine 655 is completely buried, and was the only cysteine residue we did not change. In summary, the cysteine-light myosin-II sequence was designed with the following substitutions: C49S, C312Y, C442S, C470I, C599L, C678Y.

Cysteine-Light Myosin-II is Functional In Vivo and In Vitro

Dictyostelium cells that are missing the myosin-II gene are unable to divide in suspension, and instead become large and multinucleate before eventually lysing (De Lozanne and Spudich, 1987; Knecht and Loomis, 1987). Thus, transformation of a mutant myosin-II gene into these myosin-II null cells provides a robust assay for in vivo function—assaying for rescue of the growth in suspension defect. Myosin-II null cells transformed with a plasmid encoding either a wild-type or a cysteine-light

myosin-II gene were assayed for growth in suspension. The cysteine-light myosin completely rescued the cytokinesis defect of the myosin-II null host strain (Figure 2). This is a very stringent test of myosin-II function, and we conclude that none of the cysteines that were mutagenized are essential. A cysteine-light myosin-II harboring the mutation A250C (to facilitate acceptor labeling for FRET) also completely rescued the cytokinesis defect of the myosin-II null strain (data not shown).

The S1 portion of the cysteine-light myosin-II gene was subcloned into another plasmid to facilitate the expression of an S1 that was tagged at the carboxy terminus of the heavy chain with a 6×His tag. Cysteine-light S1 was expressed, purified, and assayed for basal and actin-activated ATPase activity in vitro. The actin-activated ATPase activity of the cysteine-light S1 was very similar to that of wild-type S1 (1.0 s^{-1}), and was higher than the respective basal rate (the rate in the absence of actin). Therefore, the cysteine-light S1 retains actin-activation of its ATPase. The basal rate of the cysteine-light S1 ATPase was about 2-fold higher than that of the wild-type enzyme (0.40 s^{-1} versus 0.17 s^{-1}), suggesting that the rate-limiting phosphate release step is not as well gated as for the wild-type S1.

In summary, the cysteine-light myosin-II is a functional motor both in vivo and in vitro. It should serve as a useful starting point for future structure-function studies involving site specific chemical modification, such as disulfide cross-linking and spectroscopic probe labeling, of the protein.

FRET Strategy

Starting from the cysteine-light S1 gene described above, we generated S1 heavy chains and regulatory light chains with single reactive cysteines positioned such that, according to models based on crystallographic structures, the intercysteine distance would decrease from $\sim 75 \text{ \AA}$ to $\sim 25 \text{ \AA}$ during the poststroke to prestroke transition (Rayment et al., 1993; Dominguez et al., 1998) (Figure 1). Recombinant *E. coli* expressed *Dictyostelium* regulatory light chain (RLC) was donor labeled with Oregon green 488 maleimide at either residue 114 or 116, and then exchanged onto a recombinant *Dictyostelium* expressed S1 whose heavy chain had been previously acceptor labeled at residue 250 with tetramethylrhodamine-5-maleimide. Averaging the measured FRET distances obtained from S1 labeled with the donor dye at two different residues decreases the uncertainty due to potential constraints on the relative orientation of a given donor-acceptor dye pair (Stryer, 1978). The doubly labeled S1s were designated as $D_{114}A_{250}$ and $D_{116}A_{250}$, respectively. S1s lacking either the donor or the acceptor dye (designated as D_{114} , D_{116} , and A_{250}) were generated as controls. A common concern in applying FRET to study protein structure involves the challenge of specifically labeling one site with a donor dye, and the other site with an acceptor dye, without cross contamination of the two labeling sites. The ability to label the heavy chain and RLC separately, and then form a complex after labeling has been completed, allows this problem to be solved. A specific concern in applying FRET to discriminate between prestroke and poststroke structures (as seen in crystallographic models; see prestroke state A versus poststroke state in

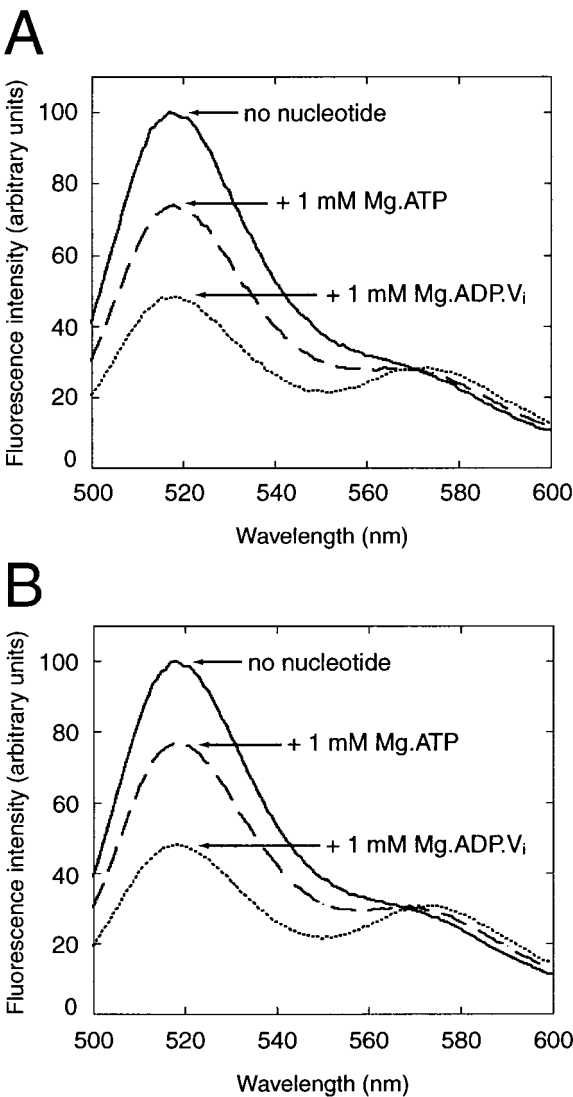


Figure 3. Steady-State FRET Emission Spectra
Spectra were taken with no nucleotides, then after the addition of Mg.ATP, and finally after the addition of Mg.ADP.V_i. The addition of Mg.ATP induces only about half as much FRET as the addition of Mg.ADP.V_i.
(A) Emission spectra of D₁₁₄A₂₅₀.
(B) Emission spectra of D₁₁₆A₂₅₀.

Figure 1) is that these two conformations, when superimposed using their catalytic domains, are pseudosymmetric about an axis that bisects the angle made by the lever arm in the two conformations. Placement of an acceptor dye near this axis of pseudosymmetry would lead to only a very small change in the FRET efficiency in transiting from the poststroke to the prestroke structure. In fact, this observation explains why when one

FRET dye is placed on the so-called SH1 native cysteine (C707 in the chicken sequence) or in the nucleotide binding site, then only a small change in FRET efficiency is measured upon addition of nucleotides and nucleotide analogs, since both locations lie near the axis of pseudosymmetry (Xiao and et al., 1998; Palm et al., 1999). We placed the acceptor dye as far as possible from this axis, at an introduced cysteine on position 250, in order to maximize the sensitivity of the FRET efficiency to a rotation in the lever arm angle.

Bound Mg.ADP.P_i Biases Myosin toward Prestroke States Much More Than Does Bound Mg.ATP

In the steady-state, *Dictyostelium* S1 in the presence of saturating amounts of Mg.ATP exists primarily as a mixture of S1.Mg.ATP and S1.Mg.ADP.P_i nucleotide states (Ritchie et al., 1993). If S1.Mg.ATP occupied the same distribution of lever arm angles as S1.Mg.ADP.P_i, then the amount of steady-state FRET observed for D₁₁₄A₂₅₀ and D₁₁₆A₂₅₀ should be the same in the presence of Mg.ATP as in the presence of Mg.ADP.V_i, a Mg.ADP.P_i analog (Werber et al., 1992). The measured steady-state FRET efficiency for D₁₁₄A₂₅₀ increased from 16% in the absence of nucleotide to 36% upon addition of Mg.ATP, and further increased to 61% upon addition of Mg.ADP.V_i (Figure 3A and Table 1). For D₁₁₆A₂₅₀, the measured steady-state FRET efficiency increased from 11% in the absence of nucleotide to 32% upon addition of Mg.ATP, and further increased to 57% upon addition of Mg.ADP.V_i (Figure 3B and Table 1). Thus, Mg.ADP.V_i induces a much greater amount of steady-state FRET than does Mg.ATP. A simple model to account for this data is that S1.Mg.ATP exists primarily with a poststroke angle lever arm conformation (low FRET efficiency), while S1.Mg.ADP.P_i exists primarily with a prestroke angle lever arm conformation (high FRET efficiency). The simplest interpretation is that in the presence of Mg.ATP, D₁₁₄A₂₅₀ and D₁₁₆A₂₅₀ exist as a roughly equimolar mixture of S1.Mg.ATP and S1.Mg.ADP.P_i nucleotide states, and therefore exhibit only half the FRET efficiency as in the presence of ADP.V_i.

In the Steady-State, D₁₁₄A₂₅₀ Exists Primarily as a Mixture of S1.Mg.ATP and S1.Mg.ADP.P_i States, Just Like Wild-type S1

The above interpretation is only valid if D₁₁₄A₂₅₀ in the presence of saturating Mg.ATP exists primarily as a mixture of S1.Mg.ATP and S1.Mg.ADP.P_i states, as in the case of the wild-type S1, with the P_i-free S1.Mg.ADP state representing an insignificant part of the total population. If the rate of ADP release for D₁₁₄A₂₅₀ were slowed by >100-fold compared to wild-type S1, to the same level as the rate of P_i release, or if the P_i release rate were enhanced by >100-fold, then S1.Mg.ADP could account for nearly half of the S1 molecules in the presence of saturating Mg.ATP (Woodward et al., 1991; Ritchie et al., 1993; Woodward et al., 1995). Then the lower

Table 1. Steady State FRET Efficiencies

Nucleotide added	D ₁₁₄ A ₂₅₀ steady-state FRET efficiency	D ₁₁₆ A ₂₅₀ steady state FRET efficiency
No nucleotide	16% ± 1%	11% ± 2%
Mg.ATP	36% ± 3%	32% ± 3%
Mg.ADP.V _i	61% ± 1%	57% ± 2%

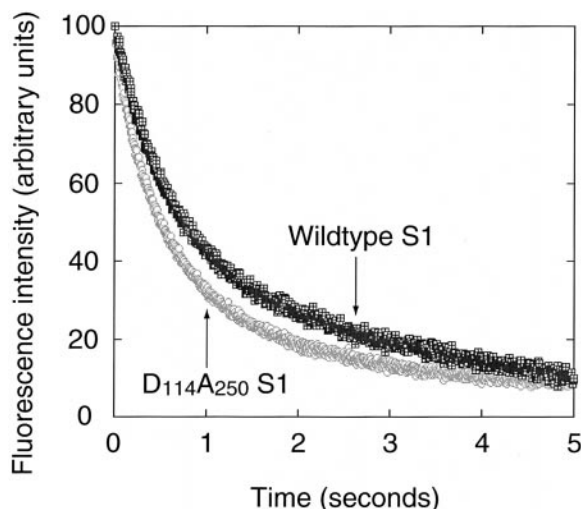


Figure 4. MantADP Release Monitored by Stopped Flow Fluorescence

S1 (0.1 μ M) was preincubated with 2.5 μ M mantADP, and the complex was mixed in the stopped-flow device with 0.4 mM ATP. Wild-type *Dictyostelium* S1 releases mantATP at 0.9 ± 0.1 s $^{-1}$, while $D_{114}A_{250}$ releases mantADP at 1.3 ± 0.1 s $^{-1}$.

FRET efficiency observed in the presence of Mg.ATP would be reflecting the poststroke configuration of the P_i -free S1.Mg.ADP population, and not of the poststroke configuration of the S1.Mg.ATP population. Conventionally, measurements of ADP release rate from myosins have involved the use of the fluorescent analog mantADP (Woodward et al., 1991; Ritchie et al., 1993; Woodward et al., 1995). We found that the rate of release of mantADP from $D_{114}A_{250}$ (1.3 ± 0.1 s $^{-1}$) is not slower than that of wild-type S1 (0.9 ± 0.1 s $^{-1}$), but is instead about 40% faster (Figure 4). With the assumption that the relative rates of mantADP release for the $D_{114}A_{250}$ and wild-type S1 reflect the relative rates of ADP release, we conclude that the ADP release rate is not significantly changed. If the P_i release rate were enhanced by >100-fold, one would expect this to be reflected in a large increase in the steady state basal ATPase activity of the $D_{114}A_{250}$ compared to wild-type S1. We found these rates to be within a factor of two (0.27 ± 0.01 s $^{-1}$ for $D_{114}A_{250}$ versus 0.17 ± 0.01 s $^{-1}$ for wild-type S1).

S1 Populates Three Lever Arm Angles, Whose Distribution Is Influenced by Nucleotides

If S1 exists as a heterogeneous mixture of conformational states, then meaningful assignment of FRET efficiencies to distances can only be made after resolving

the FRET distributions present in the sample. Steady-state fluorescence reports only on the mean FRET efficiency of the dye-pairs in solution, and gives no information regarding the distribution about that mean. We therefore measured time-resolved fluorescence in the frequency domain to recover donor lifetime distributions, from which FRET and distance distributions could be calculated (Table 2). FRET distributions are most easily extracted in the case where the donor alone control behaves as a single exponential homogeneous species. Fortunately, this was the case for both the D_{114} and D_{116} mutants (Figures 5A and 5C; Table 2). Addition of nucleotides had insignificant effects on the fitted lifetimes for the donor alone controls (Figures 5A and 5C). D_{114} phase and modulation responses (taken in the absence of nucleotides, then after the addition of Mg.ATP, and finally after the addition of Mg.ADP.V $_i$) fit well in a global analysis to a single lifetime of 4.09 ns ($\chi^2 = 6.0$), while global analysis of D_{116} responses under the same conditions fit well to a single lifetime of 4.28 ns ($\chi^2 = 8.3$). Analysis of $D_{114}A_{250}$ phase and modulation responses, taken under the same three nucleotide conditions, yielded a good three lifetime fit in global analysis ($\tau_1 = 3.95$ ns, $\tau_2 = 1.00$ ns, and $\tau_3 = 0.020$ ns) ($\chi^2 = 3.6$) (Tables 2 and 3; Figure 5B). The χ^2 for this fit remained roughly constant for τ_3 between 0–0.20 ns. The implied steady-state FRET agreed with the measured steady-state FRET when the fit was performed with τ_3 fixed at 0.020 ns. Similar results were found for the global analysis of the $D_{116}A_{250}$ responses under the same conditions ($\tau_1 = 3.93$ ns, $\tau_2 = 0.93$ ns, and $\tau_3 = 0.010$ ns) ($\chi^2 = 3.9$) (Tables 2 and 4; Figure 5D). Again, the χ^2 for this fit remained roughly constant for τ_3 between 0–0.20 ns, and the implied steady-state FRET agreed with the measured steady-state FRET when the fit was performed with τ_3 fixed at 0.010 ns.

A two component fit ($\tau_1 = 3.90$ ns and $\tau_2 = 0.76$ ns) was attempted for $D_{114}A_{250}$ and was found to be inappropriate, since the implied steady-state donor quenching was much lower than the measured steady-state donor quenching, especially for the Mg.ADP.V $_i$ data (37% implied vs. 61% measured.) Furthermore, the χ^2 for the two lifetime fit was 80% higher than for the three lifetime fit. A two component fit was attempted for $D_{116}A_{250}$ as well, but was also found to be inappropriate, as the implied steady-state FRET was in poor agreement with the measured steady-state FRET, especially for the Mg.ADP.V $_i$ data set (31% implied versus 57% measured), similar to the case with $D_{114}A_{250}$.

The observed three lifetime components for $D_{114}A_{250}$ correspond to FRET efficiencies of 3.4%, 76%, and 99.5%. These FRET efficiencies indicate apparent FRET distances of 93 Å, 44 Å, and 22 Å, respectively. The

Table 2. Donor Lifetimes, FRET Efficiencies, and Distance Distributions

S1	Fitted donor lifetime	FRET efficiency	Distance
D_{114}	4.09 \pm 0.01 ns		
$D_{114}A_{250}$	3.95 \pm 0.02 ns	3.4 \pm 0.8%	93 \pm 4 Å
	1.00 \pm 0.02 ns	76 \pm 1%	43.7 \pm 0.4 Å
	0.020 \pm 0.002 ns	99.5 \pm 0.1%	21.9 \pm 0.8 Å
D_{116}	4.28 \pm 0.02 ns		
$D_{116}A_{250}$	3.93 \pm 0.02 ns	8.2 \pm 0.9%	79 \pm 2 Å
	0.93 \pm 0.04 ns	78 \pm 1%	42.9 \pm 0.4 Å
	0.010 \pm 0.003 ns	99.8 \pm 0.1%	18.8 \pm 1.7 Å

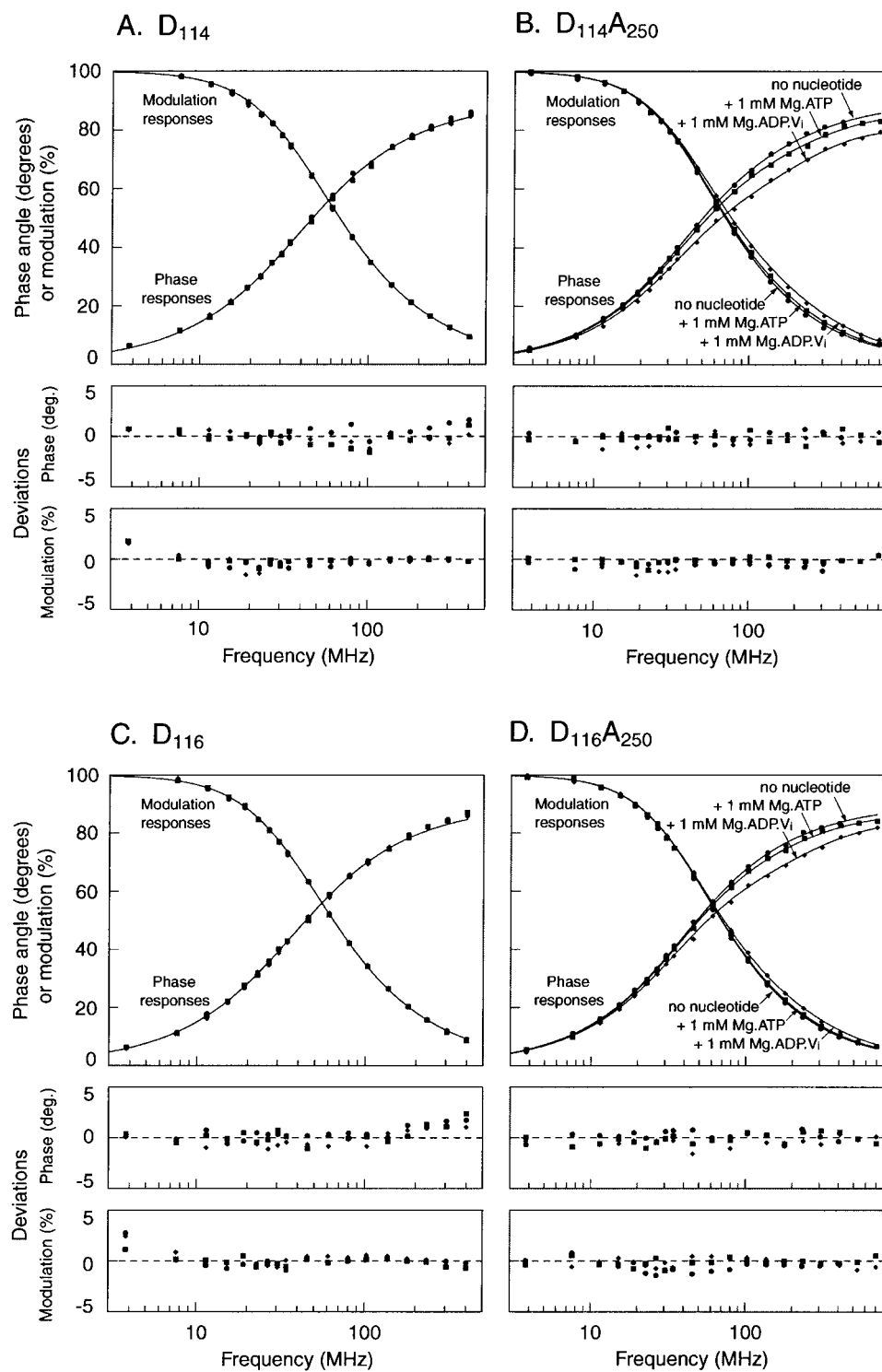


Figure 5. Frequency Domain Time-Resolved Fluorescence Spectra

Phase and modulation responses with no nucleotides (circles), in the presence of Mg.ATP (squares), and in the presence of Mg.ADP.Vi (diamonds) measured over a frequency range of 4 to 700 MHz.

(A) Phase and modulation responses of D_{114} .

(B) Phase and modulation responses of $D_{114}A_{250}$.

(C) Phase and modulation responses of D_{116} .

(D) Phase and modulation responses of $D_{116}A_{250}$.

Table 3. $D_{114}A_{250}$ Donor Lifetime Mole Fractions

$D_{114}A_{250}$ donor lifetime	No nucleotide mole fraction	Mg.ATP mole fraction	Mg.ADP.V _i mole fraction
3.95 ns	0.67	0.41	0.10
1.00 ns	0.10	0.17	0.23
0.020 ns	0	0.19	0.44

0.23 mole fraction fixed at 4.09 ns, to account for 77% acceptor labeling efficiency.

analysis of the $D_{116}A_{250}$ data yielded FRET efficiencies of 8%, 78%, and 99.8%, corresponding to distances of 79 Å, 43 Å, and 19 Å, respectively. Shorter distances imply more prestroke-like angle of the lever arm. The remarkable agreement between the FRET distances reported from $D_{114}A_{250}$ and $D_{116}A_{250}$ suggests that there are no significant errors due to unique donor-acceptor inter-dye orientational restrictions.

Updated Model: Bound Mg.ADP.P_i Biases Myosin Toward Two Distinct Prestroke States Much More Than Does Bound Mg.ATP

The simple model presented in the previous section proposes that addition of Mg.ADP.V_i induces a large fraction of S1 heads to adopt a prestroke angle, and addition of Mg.ATP induces only half as many heads to adopt a prestroke angle. The time-resolved data requires this simple model to be revised, however, to include two prestroke angle states, as opposed to just one (Tables 3 and 4). Taken together, the steady-state and time-resolved data support the model shown in Figure 6, where Mg.ATP hydrolysis is more responsible for population of prestroke configurations than is Mg.ATP binding. Thus, S1 can discriminate between Mg.ATP and Mg.ADP.P_i.

This result is novel in showing that a functional myosin motor in the S1.Mg.ATP nucleotide state exists primarily with a poststroke state angle of the lever arm. An advantage of this study is that it did not require inference from experiments with presumed ATP analogs (such as ADP.BeF₃) or ATPase cycle arresting mutants, but rather reported on the conformation of working motors turning over ATP in solution. The question of the relative roles of ATP and ADP.P_i in priming the motor has been debated for three decades. Lymn and Taylor (1971) proposed that ATP binding drives S1 from a poststroke angle, strong actin affinity state to a poststroke angle, weak actin affinity state, and that ATP hydrolysis drives the motor to a prestroke angle, weak actin affinity state. Eisenberg and Greene (1980) invoked the principle of parsimony in suggesting that a simpler two-state model would suffice, where S1 can exist only in a poststroke angle, strong actin affinity state and a prestroke angle, weak actin affinity state. ATP binding would force the myosin from the poststroke angle, strong actin affinity

state directly to the prestroke angle, weak actin affinity state. ATP hydrolysis would not be associated with any conformational changes, but rather would serve to prepare the γ -phosphate for subsequent release.

More recently, Holmes suggested that the available crystal structures were consistent with the simpler Eisenberg and Greene type model (Holmes, 1997). Furthermore, Smith and Rayment proposed that the poststroke angle crystal structure should be catalytically inactive, due to lack of positioning of the putative nucleophilic water in that structure (Rayment, 1996; Smith and Rayment, 1996). Therefore, the S1 should be able to exist in the prestroke angle conformation at least transiently if not primarily, in order to hydrolyze the ATP in a timely manner. Crystallization of myosin fragments in a prestroke angle conformation complexed with Mg.ADP.BeF₃, a supposed Mg.ATP analog, led further credence to the simple two-state model (Dominguez et al., 1998).

Suzuki and colleagues studied the conformation of the *Dictyostelium* myosin catalytic domain, a head fragment missing the light chain binding domain, using FRET between GFP on the amino terminus and BFP on the carboxy terminus (Suzuki et al., 1998). They examined this protein in the presence of ATP, using two different mutants that arrest myosin in a weak actin affinity, ATP bound state (Sasaki et al., 1998; Suzuki et al., 1998). Interestingly, the G457A mutant exhibited FRET efficiency consistent with a poststroke angle, while the E459A mutant exhibited FRET efficiency consistent with a prestroke angle. Assuming that the intact motor containing the light chain binding domain would behave in a similar manner, this result suggests that myosin in the S1.Mg.ATP state can access weak actin affinity states with both poststroke angle and prestroke angle conformations. Thus, the two-state model is at best an oversimplification, since S1 can reach a poststroke angle, weak actin affinity state. However, these mutant studies did not reveal whether the conformational equilibrium lies toward the poststroke state angle, as in the Lymn and Taylor model, or toward the prestroke state angle, more similar to the Eisenberg and Greene model, since the mutations are likely perturbing that equilibrium. Thus, our results are a significant extension of this previous work, in investigating the lever arm conformational equilibrium of the full length S1.Mg.ATP complex.

Table 4. $D_{116}A_{250}$ Donor Lifetime Mole Fractions

$D_{116}A_{250}$ donor lifetime	No nucleotide mole fraction	Mg.ATP mole fraction	Mg.ADP.V _i mole fraction
3.93 ns	0.73	0.42	0.17
0.93 ns	0.04	0.09	0.19
0.010 ns	0	0.26	0.41

0.23 mole fraction fixed at 4.28 ns, to account for 77% acceptor labeling efficiency.

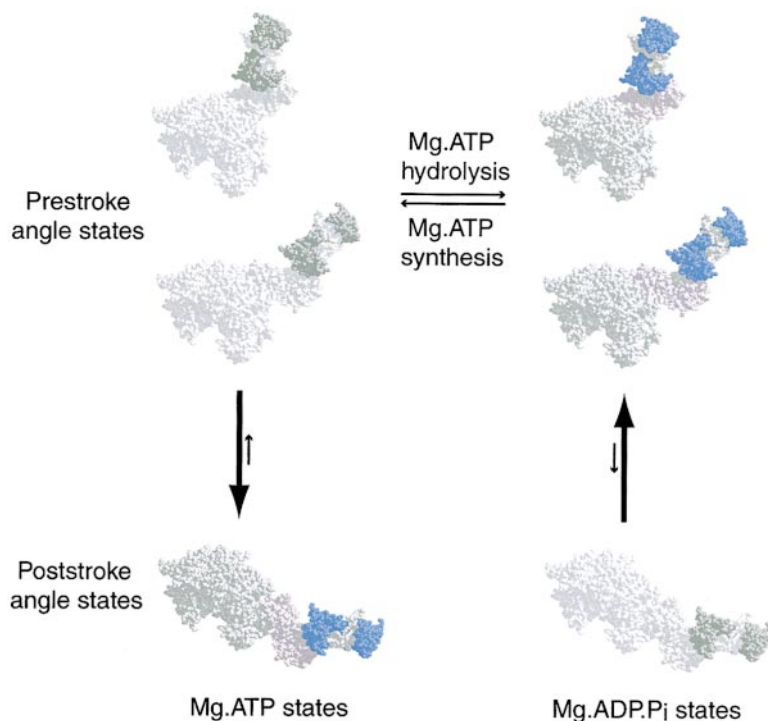


Figure 6. Conformations of S1 Bound to Mg.ATP and Mg.ADP.P_i

Structures on the left represent Mg.ATP states, and structures on the right represent Mg.ADP.P_i states. The two prestroke angle states represent prestroke state A and B in Figure 1. Structures in color are the predominant conformations that are populated in each nucleotide state.

Brust-Mascher and colleagues (1999) note that EPR studies suggest dynamic disorder in the angle between the catalytic domain and the lever arm domain in both S1.Mg.ATP and S1.Mg.ADP.P_i states. They furthermore point out that, in a muscle fiber, interactions of the lever arm domain with the myosin thick filament and interactions of the catalytic domain with the actin filament could influence the conformational equilibrium of the lever arm angle. Although we see three discrete lever arm angles and not dynamic disorder, our results are consistent with the proposed notion that the conformational equilibrium does not lie too far from unity, and that external influences can perturb that equilibrium. Even though the *Dictyostelium* S1.Mg.ATP spends most of its time in the poststroke angle conformation, it may have to transiently visit the prestroke angle conformation in order to catalyze ATP hydrolysis. Another important point is that when ATP binds to a myosin head attached to an actin filament while exerting positive tension, that tension energetically favors the S1 transiting first to a poststroke angle, weak actin affinity state, at least until the actin filament is released. Thus, this would be an example of the outside environment perturbing the lever arm conformational equilibrium of a myosin.Mg.ATP nucleotide state.

FRET Distances Compared with Crystal Structures of Myosin

Crystal structures of myosin head fragments containing the ELC have been found with different lever arm angles (Rayment et al., 1993; Dominguez et al., 1998; Houdusse et al., 1999). A prestroke state model based on the chicken smooth muscle MDE.Mg.ADP.AIF₄ structure (prestroke state A in Figure 1) predicts a distance of 25 Å from RLC-Cys₁₁₄ to HC-Cys₂₅₀ (measuring from the β carbon

positions), and a distance of 28 Å from RLC-Cys₁₁₆ to HC-Cys₂₅₀. The α carbon to β carbon vectors of the two cysteine residues generally point toward each other in the models (for both D₁₁₄A₂₅₀ and D₁₁₆A₂₅₀), and thus the distances between the dyes themselves might be expected to be shorter than the distances between the cysteines to which they are attached. The length of the dyes, measuring from the Cβ to which they are attached, is about 10 Å. Therefore, the measured FRET distances of 22 Å and 19 Å are consistent with prestroke state A.

A model based on the chicken skeletal nucleotide free S1 structure (poststroke state in Figure 1) predicts a distance of 75 Å from RLC-Cys₁₁₄ to HC-Cys₂₅₀, and a distance of 76 Å from RLC-Cys₁₁₆ to HC-Cys₂₅₀ (measuring from the β carbon positions). The average of the 93 Å and 79 Å measured FRET distances, at 86 Å, is roughly consistent with the 75 Å predicted from the chicken skeletal structure based poststroke state model. The data is more consistent with a poststroke state whose lever arm is angled further downwards, with respect to the orientation shown in Figure 1. Electron micrographic reconstructions suggest that *Dictyostelium* and smooth muscle myosin-II both have rigor states with a more downwards angle of the lever arm than the skeletal myosin-II (Rosenfeld et al., 2000), but uncertainty in distance is significant for measured FRET efficiencies below ~10%—in this case, for distances greater than ~75 Å—due in part to the R⁻⁶ dependence on the rate of FRET. Furthermore, calculations of low FRET efficiencies are also particularly sensitive to errors in the measurements of fluorescence intensity (for steady-state experiments) or lifetime (for time-resolved experiments) of the donor alone control species, as can be seen from inspection of the equation for FRET efficiency: $ET = 1 - F_{DA}/F_D = 1 - \tau_{DA}/\tau_D$. Thus, the 86 Å

measured FRET distance could be consistent with conformational states whose cysteines are predicted to be even farther apart, such as in the case with the scallop ADP bound S1 structure (Houdusse et al., 1999), where the predicted distance is 108 Å. On the other hand, if the addition of Mg.ATP to nucleotide free S1 were to cause half of the population to adopt the scallop ADP bound S1 structure, then one would expect to see the lifetime of a fraction of the signal to increase. However, this was not observed. Thus, our results suggest that the scallop ADP bound S1 structure is not the major S1.Mg.ATP conformation. Our experiment is not sensitive enough to rule out the possibility that a minority of the S1.Mg.ATP heads are in the scallop S1.ADP conformation.

An Unexpected, Novel Lever Arm Angle Induced by Bound Mg.ADP.P_i

The measured 44 Å and 43 Å FRET distances for D₁₁₄A₂₅₀ and D₁₁₆A₂₅₀, respectively, suggest yet another lever arm conformation, which we have named prestroke state B (Figure 1). A tomographic three-dimensional reconstruction of quick-frozen contracting insect flight muscle has shown three angles of the lever arm domain, of 125°, 105°, and 70° (Taylor et al., 1999). Prestroke B may be reflecting a similar conformation to the 105° lever arm angle of that study. On the other hand, the authors interpret the difference between the 125° and 105° angles as due to a rotation of the entire S1 head as a whole, and thus conclude that the angle between the catalytic domain and the lever arm domain is constant between the two structures.

What is the significance of this novel structure? One possibility is that this second prestroke state gives the S1 more flexibility in attaching to the actin filament if it approaches the actin out of register or at a bad angle. The sacrifice is that if the S1 attaches in prestroke state B, then the resulting powerstroke will cover a shorter distance than had the S1 attached in prestroke state A. Thus in this model, maximum stepsize is no longer guaranteed, but the increased flexibility allows for a greater chance for a productive attachment to nearby actin filaments. Thomas and colleagues have proposed a similar model, termed the disorder-to-order transition mechanism for force generation (Roopnarine et al., 1998). Comparison of EPR spectra from muscle fiber myosin heads labeled at SH1 versus those labeled on the RLC has led to the interpretation that the angle between the catalytic domain and the lever arm domain is dynamically disordered on the microsecond time scale in the S1.Mg.ATP and S1.Mg.ADP.P_i states (Roopnarine et al., 1998). Our FRET evidence, on the other hand, suggests two discrete angles of the lever arm with respect to the catalytic domain that are visited in the S1.Mg.ADP.P_i state (the presumptive prestroke nucleotide state). Both models are similar, though, in that they suggest that there is more than one prestroke state angle.

A further implication of this discovery of a novel myosin lever arm conformation is that the list of stable lever arm angles that are being detected experimentally is growing. It is conceivable that all myosins execute their powerstroke through multiple steps, in the sense that

the lever arm may rest transiently at discrete intermediate lever arm angles. These intermediate angles, if they exist, might be stabilized mechanically through the influence of optical tweezers. Alternatively, these intermediate angles may be stabilized by mutations to the myosin motor which effectively slow down different parts of the ATPase cycle.

In summary, these experiments demonstrate a dramatic change in orientation of the myosin-II lever arm upon hydrolysis of ATP. These solution studies fit well with various crystallographic states previously observed. In addition, we have described a high resolution sensor of lever arm angle that can be used to examine not only the effects of binding various nucleotides to the active site of myosin, but also how a wide variety of myosin mutations affect the myosin-II structure.

Experimental Procedures

Protein Engineering and Preparation

Subcloning procedures were carried out using standard protocols (Sambrook et al., 1989). The cysteine-light *Dictyostelium* myosin-II S1 gene fragment, containing the mutations (C49S, C312Y, C442S, C470I, C599L, and C678Y), was generated using splice-overlap extension PCR mutagenesis (Ho et al., 1989), and was spliced into a full-length *Dictyostelium* myosin-II gene in the expression vector pTIKL-Myo. The introduced mutations were verified by dideoxyDNA sequencing. The S1 gene fragment was then subcloned into pTIKLOES1, an expression vector for producing S1 with a carboxy terminal 6×His tag on the heavy chain. The mutation A250C was introduced into the cysteine-light S1 gene sequence via splice overlap extension PCR mutagenesis. The newly created gene was then subcloned back into pTIKLOES1 to facilitate S1 expression. The introduced mutation was verified by dideoxyDNA sequencing.

Dictyostelium S1 6×His was expressed in *Dictyostelium* AX3-ORF+ cells (grown in suspension) and purified as described (Giese and Spudich, 1997). The *Dictyostelium* RLC gene was synthesized from 40-mer oligonucleotides to incorporate *E. coli* codon bias into the DNA sequence (Stemmer et al., 1995). A 6×His sequence was inserted into the beginning of the RLC gene to facilitate purification. A 6×Arg sequence was appended to the end of the RLC gene as well. Two RLC mutant genes were constructed, containing the mutations (C49L and L114C) or (C49L and K116C), respectively. The RLC was expressed in *E. coli*, purified by Ni-NTA chromatography in the presence of 7 M GuCl, and refolded by dialysis against 25 mM HEPES (pH 7.0), 150 mM NaCl, 1 mM EDTA, and 0.1 mM Tris (2-carboxyethyl) phosphine (TCEP).

Dictyostelium Manipulations

The full-length myosin-II gene encoding plasmids were electroporated into HS1, a myosin-II null strain of *Dictyostelium discoideum* (Ruppel et al., 1994), while the S1 gene encoding plasmids were electroporated into AX3-ORF+ cells (Manstein et al., 1995), as described previously (Egelhoff et al., 1991). Transformants were selected for and maintained in DD HL5 media containing 8 mg/ml G418 (Gibco, BRL), 100 units/ml penicillin, and 100 µg/ml streptomycin. Growth curves were generated by measuring cell number of aliquots in a hemacytometer over the course of six days, with at least one time point per day, of cells in a 25 ml volume in a 125 ml Erlenmeyer flask, shaking at 200 rpm at 22°C, inoculated with a starting density of about 10⁴ cells/ml.

Labeling and RLC Exchange

A suspension of 20 µM RLC, 25 mM HEPES (pH 7.0), 300 mM NaCl, 1 mM EDTA, 0.025 mM TCEP, and 25 µM Oregon green 488 maleimide (Molecular Probes) was incubated at 22°C for 1 min, and the reaction was quenched by the addition of 1 mM DTT. Meanwhile, a suspension of 1 µM S1, 25 mM HEPES (pH 7.0), 25 mM NaCl, 10 mM MgCl₂, and 0.1 mM TCEP was mixed with 0.05× volume 1 M

HEPES (pH 4.2), and incubated for 1 min. Then tetramethylrhodamine-5-maleimide (Molecular Probes) was added to a final concentration of 20 μ M, and the reaction proceeded for 1 min before quenching with DTT at a final concentration of 1 mM. The S1 mixture was neutralized with the addition of 0.075 \times volume 1 M HEPES (pH 7.4). The S1 was mixed with a final concentration of 3 μ M F actin for 30 min at 22°C. The F actin S1 was pelleted by centrifugation at 8000 \times g and resuspended in 25 mM HEPES (pH 7.0), 300 mM NaCl, 10 mM MgCl₂, and 1 mM DTT, centrifuged at 8000 \times g, and resuspended. The labeled S1, bound to actin, and RLC were mixed together and incubated at 22°C for 1 hr. The exchanged S1 F actin was pelleted and resuspended in 25 mM HEPES (pH 7.0), 300 mM NaCl, 10 mM MgCl₂, and 1 mM DTT. The material was pelleted and resuspended in 25 mM HEPES (pH 7.0), 25 mM NaCl, 10 mM MgCl₂, 1 mM DTT, and 2 mM ADP. This process was repeated three more times. The pellet was resuspended in 25 mM HEPES (pH 7.0), 150 mM NaCl, 1 mM EDTA, 10 mM ATP, and 1 mM DTT and centrifuged. The supernatant was collected, and the extraction was repeated. A final concentration of 10 mM MgCl₂ was added to the supernatant, incubated for 10 min at 22°C, and the sample was centrifuged at 10000 \times g. The resulting supernatant was dialyzed against 25 mM HEPES (pH 7.0), 150 mM NaCl, 2 mM MgCl₂, and 0.1 mM TCEP. The dialyzed protein was frozen in liquid nitrogen and thawed prior to use. After thawing, the protein was centrifuged at 10000 \times g just before use. Acceptor labeling was measured on A₂₅₀, the S1 control lacking the donor dye, by comparing absorbance at 280 nm with absorbance at 554 nm, using $\epsilon_{280} = 0.8 \text{ M}^{-1}\text{cm}^{-1}$ for S1 (Ritchie et al., 1993), $\epsilon_{280} = 14,000 \text{ M}^{-1}\text{cm}^{-1}$, and $\epsilon_{554} = 95,000 \text{ M}^{-1}\text{cm}^{-1}$ (Molecular Probes) for the attached acceptor dye. The acceptor labeling was calculated as 0.92 acceptor dyes per S1. Acceptor labeling for the control S1 lacking the A250C mutation was measured to be 0.15 acceptor dyes per S1. Thus, the Cys₂₅₀ specific labeling was calculated to be 0.77 acceptor dyes per S1.

Steady-State Fluorescence Measurements

Steady-state fluorescence was measured with an SLM-Aminco-Bowman Series 2 luminescence spectrometer. Solutions contained 25 mM HEPES (pH 7.0), 150 mM NaCl, 2 mM MgCl₂, 0.1 mM TCEP at 20°C, and 0.2 μ M S1. The dyes were excited at 490 nm, and donor emission was read out at 518 nm, where no appreciable acceptor fluorescence occurs. FRET efficiencies were calculated from donor quenching as $1 - F_{da}/F_d$, where F_{da} is the fluorescence of the donor and acceptor labeled sample and F_d is the fluorescence of the donor only labeled sample. Fluorescence intensities were normalized according to fluorescence in the presence of 0.5% SDS, where the RLC is dissociated from the HC (Smyczynski and Kasprzak, 1997). Distance between the dyes was calculated using the Forster equation (Stryer, 1978), where $R = R_0 (1/E - 1)^{1/6}$. R_0 is the Forster distance, and was calculated as $R_0 = [(8.79 \times 10^{-5}) J \kappa^2 n^{-4} \phi_D]$, where J is the overlap integral between the donor and acceptor dyes attached to the S1, expressed in $\text{M}^{-1}\text{cm}^{-1}\text{nm}^{-4}$ ($J = 3.1 \times 10^{15}$ for both D₁₁₄A₂₅₀ and D₁₁₆A₂₅₀), κ^2 is the orientation factor (assumed to be 0.667), n is the refractive index (assumed to be 1.4), and ϕ_D is the quantum yield measured as 0.68 for D114 and 0.73 for D116, using disodium fluorescein in 0.01 M NaOH as a reference ($\phi_D = 0.91$) (Heidecker et al., 1995). The calculated R_0 was 53 Å for both D₁₁₄A₂₅₀ and D₁₁₆A₂₅₀. Measurements were taken for the no nucleotide condition, then 1 mM Mg.ATP final concentration was added, and measurements taken again, then 1 mM Mg.ADP.V_i final concentration was added, the sample incubated at 20°C for 10 min, and measurements were taken a final time. The same energy transfer efficiencies were measured for samples when the S1.Mg.ADP.V_i was assayed directly (no Mg.ATP added).

Steady-State ATPase Measurements

ATPase activities for the wild-type and cysteine-light myosin-II S1 were determined at 30°C by measuring the rate of release of labeled P_i using [γ -³²P]ATP in a TLC assay as described by Giese and Spudich (1997). The buffer conditions used were 25 mM imidazole (pH 7.4), 25 mM KCl, 4 mM MgCl₂, 1 mM DTT, 3 mM ATP, and 0.2–1 μ M S1. Actin-activated ATPase was measured in the presence of 50 μ M F actin, which was prepared as previously described (Pardee

and Spudich, 1982). Curves were fit to the Michaelis-Menten equation using Kaleidograph (Abelbeck Software). We used a PK/LDH-linked ATPase assay to measure the ATPase rate of D₁₁₄A₂₅₀ and wild-type S1 at 20°C (Furch et al., 1998). The buffer conditions used were the same as for the FRET fluorescence measurements (25 mM HEPES [pH 7.0], 150 mM NaCl, 2 mM MgCl₂, and 0.1 mM TCEP at 20°C). NADH oxidation was observed using fluorescence (excitation at 340 nm, emission at 450 nm). Samples contained 1 mM DTT, 0.1 mM NADH, 0.25 mM PEP, 10 units/ml lactate dehydrogenase, and 12 units/ml pyruvate kinase.

Stopped-Flow Fluorometry

Stopped-flow experiments were performed as described (Murphy and Spudich, 1999) on a DX.17MV sequential stopped-flow fluorometer (Applied Photophysics, Leatherhead, UK). Illumination was generated with a Hamamatsu mercury-xenon lamp (Middlesex, NJ) and passed through an Applied Photophysics SpectraKinetic monochromator. The release of 2'(3')-O-(N-methylanthraniloyl) ADP (mantADP) was followed by measurement of fluorescence excited at 290 nm and collected through a KV 380 nm filter. Data was analyzed by a least-squares fitting procedure (Kaleidograph). Assays were carried out under the same buffer conditions as for the FRET fluorescence measurements (25 mM HEPES [pH 7.0], 150 mM NaCl, 2 mM MgCl₂, and 0.1 mM TCEP at 20°C). To measure the off-rate of mantADP, 0.1–0.2 μ M S1 (final) was premixed with 1.3 μ M mantADP (final), and then the complex was rapidly mixed with 0.2 mM Mg.ATP (final), after which the mant fluorescence decrease was measured over time.

Time-Resolved Fluorescence Measurements and Data Fitting

Fluorescence lifetimes were measured using a frequency-domain 10 GHz fluorometer equipped with a Hamamatsu 6 min microchannel plate detector (MCP-PMT) as previously described (Laczko et al., 1990). The instrument covered a wide frequency range (4–5000 MHz), which allowed detection of lifetimes ranging from several nanoseconds to a few picoseconds. Samples were placed in a 2 mm path-length cuvette. The excitation was provided by the frequency-doubled output of a cavity-dumped pyridine-2 dye laser tuned at 385 nm synchronously pumped by a mode-locked argon ion laser. Sample emission was filtered through an ORIEL interference filter centered at 520 nm (10 nm bandwidth) together with CORNING 3-72 and 4-96 filters. This filter combination reinsured that excitation light and acceptor fluorescence would not contribute to the observed donor fluorescence. For the reference signal, DCS in methanol (463 ps fluorescence lifetime) (Laczko et al., 1990) was observed through the same filter combination. Samples under the same conditions as the steady-state fluorescence experiments outlined above were used for the time-resolved experiments (25 mM HEPES [pH 7.0], 150 mM NaCl, 2 mM MgCl₂, and 0.1 mM TCEP at 20°C). Measurements were taken for the no nucleotide condition, then 1 mM Mg.ATP final concentration was added, and measurements taken again, then 1 mM Mg.ADP.V_i final concentration was added, the sample incubated at 20°C for 10 min, and measurements were taken a final time. The governing equations for the time-resolved intensity decay data were assumed to be a sum of discrete exponentials as in $I(t) = \sum \alpha_i \exp(-t/\tau_i)$, where $I(t)$ is the intensity decay, α_i is the amplitude (preexponential factor), and τ_i the fluorescence lifetime of the i -th discrete component. Fractional intensity, amplitude, and lifetime parameters were recovered by a nonlinear least squares procedure using the CFS software (Lakowicz et al., 1987).

Model Building

Prestroke state A in Figure 1 was built by combining the *Dictyostelium* ADP.V_i catalytic domain (Smith and Rayment, 1996), the MDE.ADP.AIF₄ converter and ELC binding domain (Dominguez et al., 1998), and the RLC binding portion of the lever arm from the skeletal S1 structure (Rayment et al., 1993), using superposition of the ELC between the latter two models for proper alignment. The dyes were modeled into the structure using InsightII (Molecular Simulations, Inc.). The poststroke state in Figure 1 was built by combining the same *Dictyostelium* catalytic domain described above with the converter and lever arm from the skeletal S1 structure (Rayment et al., 1993). Prestroke state B in Figure 1 is a model to fit the 44 Å

measured FRET distance by rigid body translation and rotation of the lever arm domain.

Acknowledgments

We thank Wen Liang for measuring *Dictyostelium* growth rates. This work was supported by NIH grant AR42895 to J. A. S. and NIH grants RR-08110 and GM-35154 (to J. R. L.). W. M. S. was supported by a Howard Hughes Medical Institute Predoctoral Fellowship.

Received March 7, 2000; revised July 10, 2000.

References

- Brust-Mascher, I., LaConte, L.E., Baker, J.E., and Thomas, D.D. (1999). Myosin light-chain domain rotates upon muscle activation but not ATP hydrolysis. *Biochemistry* 38, 12607–12613.
- Burmeister-Getz, E., Cooke, R., and Selvin, P.R. (1998). Luminescence resonance energy transfer measurements in myosin. *Biophys. J.* 74, 2451–2458.
- Cooke, R. (1986). The mechanism of muscle contraction. *CRC Crit. Rev. Biochem.* 21, 53–118.
- Corrie, J.E., Brandmeier, B.D., Ferguson, R.E., Trentham, D.R., Kendrick-Jones, J., Hopkins, S.C., van der Heide, U.A., Goldman, Y.E., Sabido-David, C., Dale, R.E., et al. (1999). Dynamic measurement of myosin light-chain-domain tilt and twist in muscle contraction. *Nature* 400, 425–430.
- Dayhoff, M.O. (1978). *Atlas of Protein Sequence and Structure*, Volume 5 (Washington, D.C.: National Biomedical Research Foundation).
- De Lozanne, A., and Spudich, J.A. (1987). Disruption of the *Dictyostelium* myosin heavy chain gene by homologous recombination. *Science* 236, 1086–1091.
- Dominguez, R., Freyzon, Y., Trybus, K.M., and Cohen, C. (1998). Crystal structure of a vertebrate smooth muscle myosin motor domain and its complex with the essential light chain: visualization of the pre-power stroke state. *Cell* 94, 559–571.
- Egelhoff, T.T., Titus, M.A., Manstein, D.J., Ruppel, K.M., and Spudich, J.A. (1991). Molecular genetic tools for study of the cytoskeleton in *Dictyostelium*. *Methods Enzymol.* 196, 319–334.
- Eisenberg, E., and Greene, L.E. (1980). The relation of muscle biochemistry to muscle physiology. *Ann. Rev. Physiol.* 42, 293–309.
- Fisher, A.J., Smith, C.A., Thoden, J.B., Smith, R., Sutoh, K., Holden, H.M., and Rayment, I. (1995). X-ray structures of the myosin motor domain of *Dictyostelium discoideum* complexed with MgADP.BeF₃ and MgADP.AIF₄. *Biochemistry* 34, 8960–8972.
- Furch, M., Geeves, M.A., and Manstein, D.J. (1998). Modulation of actin affinity and actomyosin adenosine triphosphatase by charge changes in the myosin motor domain. *Biochemistry* 37, 6317–6326.
- Giese, K.C., and Spudich, J.A. (1997). Phenotypically selected mutations in myosin's actin binding domain demonstrate intermolecular contacts important for motor function. *Biochemistry* 36, 8465–8473.
- Goldman, Y.E. (1998). Wag the tail: structural dynamics of actomyosin. *Cell* 93, 1–4.
- Ho, S.N., Hunt, H.D., Horton, R.M., Pullen, J.K., and Pease, L.R. (1989). Site-directed mutagenesis by overlap extension using the polymerase chain reaction. *Gene* 77, 51–59.
- Heidecker, M., Yan-Marriott, Y., and Marriott, G. (1995). Proximity relationships and structural dynamics of the phalloidin binding site of actin filaments in solution and on single actin filaments on heavy meromyosin. *Biochemistry* 34, 11017–11025.
- Holmes, K.C. (1997). The swinging lever-arm hypothesis of muscle contraction. *Curr. Biol.* 7, R112–R118.
- Holmes, K.C., Popp, D., Gebhard, W., and Kabsch, W. (1990). Atomic model of the actin filament. *Nature* 347, 44–49.
- Houdusse, A., Kalabokis, V.N., Himmel, D., Szent-Gyorgyi, A.G., and Cohen, C. (1999). Atomic structure of scallop myosin subfragment S1 complexed with MgADP: a novel conformation of the myosin head. *Cell* 97, 459–470.
- Huxley, H.E. (1969). The mechanism of muscular contraction. *Science* 164, 1356–1365.
- Huxley, A.F. (1998). Muscle: support for the lever arm. *Nature* 396, 317–318.
- St. Irving, M., Claire-Allen, T., Sabido-David, C., Craik, J.S., Brandmeier, B., Kendrick-Jones, J., Corrie, J.E., Trentham, D.R., and Goldman, Y.E. (1995). Tilting of the light-chain region of myosin during step length changes and active force generation in skeletal muscle. *Nature* 375, 688–691.
- Jontes, J.D., Wilson-Kubalek, E.M., and Milligan, R.A. (1995). A 32 degree tail swing in brush border myosin I on ADP release. *Nature* 378, 751–753.
- Kabsch, W., Mannherz, H.G., Suck, D., Pai, E.F., and Holmes, K.C. (1990). Atomic structure of the actin: DNase I complex. *Nature* 347, 37–44.
- Knecht, D.A., and Loomis, W.F. (1987). Antisense RNA inactivation of myosin heavy chain gene expression in *Dictyostelium discoideum*. *Science* 236, 1081–1086.
- Laczko, G., Gryczynski, I., Gryczynski, Z., Wiczak, W., Malak, H., and Lakowicz, J.R. (1990). A 10-GHz frequency-domain fluorometer. *Rev. Sci. Instrum.* 61, 2331–2337.
- Lakowicz, J.R., Cherek, H., Gryczynski, I., Joshi, N., and Johnson, M.L. (1987). Analysis of fluorescence decay kinetics measured in the frequency domain using distributions of decay times. *Biophys. Chem.* 28, 35–50.
- Lymn, R.W., and Taylor, E.W. (1971). Mechanism of adenosine triphosphate hydrolysis of actomyosin. *Biochemistry* 10, 4617–4624.
- Manstein, D.J., Ruppel, K.M., and Spudich, J.A. (1989). Expression and characterization of a functional myosin head fragment in *Dictyostelium discoideum*. *Science* 246, 656–658.
- Murphy, C.T., and Spudich, J.A. (1999). The sequence of the myosin 50K–20K loop affects myosin's affinity for actin throughout the actin-myosin ATPase cycle and its maximum ATPase activity. *Biochemistry* 38, 3785–3792.
- Palm, T., Sale, K., Brown, L., Li, H., Hambly, B., and Fajer, P.G. (1999). Intradomain distances in the regulatory domain of the myosin head in prepower and postpower stroke states: fluorescence energy transfer. *Biochemistry* 38, 13026–13034.
- Pardee, J.D., and Spudich, J.A. (1982). Purification of muscle actin. *Methods Cell Biol.* 24, 271–289.
- Rayment, I. (1996). The structural basis of the myosin ATPase activity. *J. Biol. Chem.* 271, 15850–15853.
- Rayment, I., Holden, H.M., Whittaker, M., Yohn, C.B., Lorenz, M., Holmes, K.C., and Milligan, R.A. (1993). Structure of the actin-myosin complex and its implications for muscle contraction. *Science* 261, 58–65.
- Rayment, I., Rypniewski, W.R., Schmidt-Base, K., Smith, R., Tomchick, D.R., Benning, M.M., Winkelmann, D.A., Wesenberg, G., and Holden, H.M. (1993). Three-dimensional structure of myosin subfragment-1: a molecular motor. *Science* 261, 50–58.
- Ritchie, M.D., Geeves, M.A., Woodward, S.K., and Manstein, D.J. (1993). Kinetic characterization of a cytoplasmic myosin motor domain expressed in *Dictyostelium discoideum*. *Proc. Natl. Acad. Sci. USA* 90, 8619–8623.
- Roopnarine, O., Szent-Gyorgyi, A.G., and Thomas, D.D. (1998). Microsecond rotational dynamics of spin-labeled myosin regulatory light chain induced by relaxation and contraction of scallop muscle. *Biochemistry* 37, 14428–14436.
- Rosenfeld, S.S., Xing, J., Whitaker, M., Cheung, H.C., Brown, F., Wells, A., Milligan, R.A., and Sweeney, H.L. (2000). Kinetic and spectroscopic evidence for three actomyosin:ADP states in smooth muscle. *J. Biol. Chem.*, in press.
- Ruppel, K.M., Uyeda, T.Q., and Spudich, J.A. (1994). Role of highly conserved lysine 130 of myosin motor domain. In vivo and in vitro characterization of site specifically mutated myosin. *J. Biol. Chem.* 269, 18773–18780.
- Sambrook, J., Fritsch, E.F., and Maniatis, T. (1989). *Molecular Cloning: A Laboratory Manual*, 2nd Edition (Plainview, NY: Cold Spring Harbor Laboratory Press).

- Sasaki, N., Shimada, T., and Sutoh, K. (1998). Mutational analysis of the switch II loop of *Dictyostelium* myosin II. *J. Biol. Chem.* 273, 20334–20340.
- Schroder, R.R., Manstein, D.J., Jahn, W., Holden, H., Rayment, I., Holmes, K.C., and Spudich, J.A. (1993). Three-dimensional atomic model of F-actin decorated with *Dictyostelium* myosin S1. *Nature* 364, 171–174.
- Sellers, J.R., and Goodson, H.V. (1995). *Motor Proteins 2: Myosin*, Volume 2, P. Sheterline, ed. (London: Academic Press Limited).
- Smith, C.A., and Rayment, I. (1996). X-ray structure of the magnesium(II).ADP.vanadate complex of the *Dictyostelium discoideum* myosin motor domain to 1.9 Å resolution. *Biochemistry* 35, 5404–5417.
- Smyczynski, C., and Kasprzak, A.A. (1997). Effect of nucleotides on the orientation of the light chain-binding domain in myosin subfragment 1. *Biochemistry* 36, 13201–13207.
- Spudich, J.A. (1994). How molecular motors work. *Nature* 372, 515–518.
- Stemmer, W.P., Cramer, A., Ha, K.D., Brennan, T.M., and Heyneker, H.L. (1995). Single-step assembly of a gene and entire plasmid from large numbers of oligodeoxyribonucleotides. *Gene* 164, 49–53.
- Stryer, L. (1978). Fluorescence energy transfer as a spectroscopic ruler. *Annu. Rev. Biochem.* 47, 819–846.
- Suzuki, Y., Yasunaga, T., Ohkura, R., Wakabayashi, T., and Sutoh, K. (1998). Swing of the lever arm of a myosin motor at the isomerization and phosphate-release steps. *Nature* 396, 380–383.
- Taylor, K.A., Schmitz, H., Reedy, M.C., Goldman, Y.E., Franzini-Armstrong, C., Sasaki, H., Tregear, R.T., Poole, K., Lucaveche, C., Edwards, R.J., et al. (1999). Tomographic 3D reconstruction of quick-frozen, Ca^{2+} -activated contracting insect flight muscle. *Cell* 99, 421–431.
- Werber, M.M., Peyser, Y.M., and Muhrad, A. (1992). Characterization of stable beryllium fluoride, aluminum fluoride, and vanadate containing myosin subfragment-1 nucleotide complexes. *Biochemistry* 31, 7190–7197.
- Whittaker, M., Wilson-Kubalek, E.M., Smith, J.E., Faust, L., Milligan, R.A., and Sweeney, H.L. (1995). A 35 Å movement of smooth muscle myosin on ADP release. *Nature* 378, 748–751.
- Woodward, S.K., Eccleston, J.F., and Geeves, M.A. (1991). Kinetics of the interaction of 2'(3')-O-(N-methylanthraniloyl)-ATP with myosin subfragment 1 and actomyosin subfragment 1: characterization of two acto-S1-ADP complexes. *Biochemistry* 30, 422–430.
- Woodward, S.K., Geeves, M.A., and Manstein, D.J. (1995). Kinetic characterization of a cytoplasmic myosin motor domain expressed in *Dictyostelium discoideum*. *Biochemistry* 90, 8619–8623.
- Xiao, M., Li, H., Snyder, G.E., Cooke, R., Yount, R.G., and Selvin, P.R. (1998). Conformational changes between the active-site and regulatory light chain of myosin as determined by luminescence resonance energy transfer: the effect of nucleotides and actin. *Proc. Natl. Acad. Sci. USA* 95, 15309–15314.